JMEPEG (2023) 32:5689–5696
https://doi.org/10.1007/s11665-023-07950-1


1059-9495/$19.00

TECHNICAL ARTICLE

# Wettability and Reactivity of Liquid Magnesium with a Pure Silver Substrate

*S. Terlicka, N. Sobczak, J.J. Sobczak, P. Darłak, and E. Ziółkowski*

Submitted: 31 December 2022 / Accepted: 11 January 2023 / Published online: 27 February 2023

**For the first time, experimental data on the high-temperature interaction of liquid Mg with pure Ag are presented. The study was performed by the sessile drop method and capillary purification procedure. The test was carried out under isothermal conditions at 720 °C in a protective atmosphere of Ar + 5 wt.% $H_2$. The solidified couple was subjected to detailed microstructural observations by scanning electron microscopy (SEM) coupled with energy-dispersive x-ray spectroscopy (EDS). Under the used conditions, immediately after contact with the Ag substrate, liquid Mg drop showed a good wetting ($\theta_0 \sim 65°$) followed by fast spreading over the substrate in subsecond time to form the final contact angle of $\theta_f \sim 31°$.SEM/EDS analysis showed that $\theta_f$ is apparent because of a deep crater (200 $\mu$m) formed in the substrate under the drop by the dissolution of Ag in liquid Mg. SEM/EDS observations of complex structural transformations in the Mg/Ag couple due to high-temperature contact and subsequent cooling are in good agreement with the Ag-Mg phase diagram. Besides substrate dissolution, the interaction between liquid Mg and solid Ag at 720 °C is accompanied with the alloying of the Mg drop with Ag and the formation of a continuous layer of the β-AgMg phase at the Mg/Ag interface. During cooling, the chemical composition of the Mg(Ag) drop continuously changes, and this process is followed by the formation of the β-AgMg phase by secondary precipitation from Ag-saturated liquid, a partial transformation of the β-AgMg to ε′-$Ag_{17}Mg_{54}$ phase by peritectic reaction, followed by the solid-state transformation of the ε′-phase to the ε-$AgMg_3$ phase, and finally, the solidification of residual liquid in the form of the two-phase eutectic mixture of $AgMg_4$ + (Mg). The results obtained suggest that a very good wetting and fast spreading observed experimentally for the Mg/Ag couple is caused by high reactivity between liquid Mg and Ag substrate leading to the combined effect of two reactive wetting mechanisms, i.e. through dissolutive wetting and wetting through the formation of the interfacial reaction product (β-phase).**

**Keywords** capillary purification procedure, contact angle, liquid magnesium, reactivity, sessile drop method, silver, wettability

## 1. Introduction

Currently, magnesium alloys are being intensively studied as a new class of materials suitable for biodegradable implants that mimic human bone with variable and directed porosity (Ref 1). In contrast to traditional implant materials (stainless steel, titanium, and cobalt-chromium alloys), magnesium and its alloys are degraded and absorbed by the human body, which effectively avoids repeating implant removal surgeries (Ref 2-4). Magnesium alloys, compared to standard materials for biomedical applications, have a density (1.75-1.84 g/cm$^3$) similar to human bone tissue (Ref 5). Moreover, they show higher mechanical compatibility suitable for orthopedic implants, as their Young's modulus is in the range of 40–45 GPa (Ref 3, 5-9). In addition, Mg alloys exhibit excellent biocompatibility, bioactivity, and bioabsorbability without harming the human body (Ref 1). However, to successfully use such implant materials in the human body, the surface of the implant must allow the absorption of proteins and the formation of a layer in the physiological environment that will promote cell/osteoblast growth (Ref 1, 10). Hence, despite many years of research into optimizing the performance of such materials (Ref 11-15), adjustment of the corrosion rate is still a major issue standing in the way of large-scale use of Mg alloys in medicine (Ref 12).

Recently, biodegradable and biocompatible Mg alloys with Ag additives have attracted much interest due to their antibacterial and anticorrosive properties (Ref 9, 11, 16). Silver possesses antimicrobial activity, which enables faster wound healing (Ref 6, 17). In addition, Ag has been also applied to the implant surface in medical surgery to decrease the incidence of infection (Ref 6, 18-20).

Moreover, in vitro experiments (Ref 11) have shown that Mg alloy containing 4 wt.% Ag exhibits very low cytotoxicity, cytocompatibility, and promising antibacterial properties. Thus, Mg alloys with Ag additives are promising biodegradable materials, although their mechanical properties after heat treatment are moderate (Ref 6). In addition, in vivo tests have

This article is an invited submission to the *Journal of Materials Engineering and Performance* selected from presentations at the 10th International Conference on High Temperature Capillarity (HTC 2022) held September 12–16, 2022, in Kraków, Poland. It has been expanded from the original presentation. The issue was organized by Prof. Natalia Sobczak of the Polish Academy of Sciences.

**S. Terlicka** and **N. Sobczak**, Institute of Metallurgy and Materials Science, Polish Academy of Sciences, Reymonta St. 25, Krakow, Poland; and **J.J. Sobczak, P. Darłak,** and **E. Ziółkowski**, Faculty of Foundry Engineering, AGH University of Science and Technology, Reymonta St. 23, Krakow, Poland. Contact e-mail: s.terlicka@imim.pl.

shown that intramedullary nails made of Mg-2% Ag alloy, when implanted into unbroken and broken mice femurs, degraded during a time without any negative effects and stimulated bone formation (Ref 6, 21). Recent advances in silver coatings and magnesium-silver alloys in antibacterial uses have also presented good results (Ref 11, 22-24). It has also been found that a small silver addition in alloys or coatings improves cytocompatibility and cell lifetime (Ref 25, 26).

Usually, the Mg-Ag alloys and components are produced by the conventional melting of pure metals (Ref 11). Recently, it was reported that Mg-Ag components can be also manufactured by advanced liquid-assisted techniques such as additive manufacturing (AD) from metal powders (e.g. (Ref 27), as a good example of a growing interest to capitalize on additive manufacturing's unique design capabilities to advance the frontiers of medicine. For many AD processes, the wettability phenomenon taking place between dissimilar materials plays a key role. Hence, it is reasonable to study the wettability of magnesium and silver to understand the processes of these materials and their interaction and reactivity under high temperatures. This will allow us to determine the possibility of using these materials among others in medicine.

Therefore, the main objective of this work was to determine for the first time the high-temperature interaction of liquid magnesium in contact with a pure silver substrate at 720 °C. The obtained results will expand the limited knowledge of the high-temperature interactions of liquid Mg with dissimilar materials (Ref 28).

## 2. Materials and Methods

### 2.1 Wettability Experiment

The high-temperature wettability of a pure silver substrate (Innovator, 99.99 wt.%) with liquid magnesium ( ≥ 99.9 wt.%) was conducted by the sessile drop method, with the use of unique apparatus designed for high-temperature tests. This device was detailed described in our previous work (Ref 28). In order to avoid a heating history, the sessile drop test was accompanied with the non-contact heating of a couple of materials while to avoid the effect of a native oxide film on the Mg sample, the capillary purification procedure was applied (Ref 28-30). For this, the Mg rod (diameter and length of about 11 mm), freshly cleaned mechanically with sandpapers and ultrasonically in isopropanol (STANLAB, p.a.) for 10 min, was immediately placed in a graphite capillary and transported to the experimental chamber. Meanwhile, the surface of the silver substrate (a cuboid with a width of 9 mm and a thickness of 5 mm) was polished using sandpapers with a gradation of 200 to 7000 and then finished on a mechanical polisher using diamond suspensions from 3 to 1/4 $\mu$m to obtain a mirror-like surface. After polishing, the substrate sample was also cleaned in isopropanol for 20 min to remove residues from the used polishing suspensions. The use of isopropanol is a popular practice in preparing samples for high-temperature wettability tests because it evaporates during pumping and does not affect wetting behavior (28). Figure 1 shows the surface of the freshly polished Ag substrate and the Mg/Ag couple after the sessile drop test.

After placing Mg and Ag substrate in the device's measuring chamber, a vacuum of $10^{-6}$ mbar was created. Then, a flowing inert gas (mixture of Ar + 5 wt.% $H_2$) was introduced into the chamber, and when the gas pressure reached $1.10 \times 10^3$ mbar,

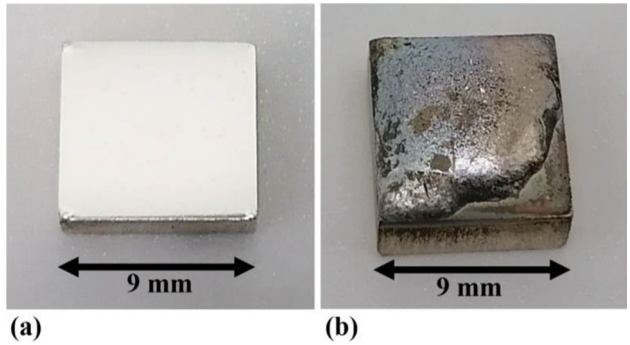


**Fig. 1** Top-view photos of the silver substrate before (a) and after (b) the sessile drop tests at 720 °C for t = 60 s under a flowing gas mixture of Ar + 5 wt.% $H_2$

the chamber was once again pumped to a vacuum of $10^{-6}$. This process was carried out to purge the chamber. After obtaining a high vacuum, isothermal heating of the capillary with Mg and Ag substrate was started to about 300 °C, in order to remove, inter alia, residual water vapor, and other volatiles from the Ag surface. Finally, the Ar + 5 wt.% $H_2$ gas was again introduced into the chamber and heating to the final test temperature ($T_{exp}$ = 720 °C) was performed. The sessile drop test was carried out in the presence of Ti chips and sponge, as well as a piece of pure Zr (99.98 wt.%), which were placed next to the Ag substrate to serve as oxygen getters (29).

A capillary purification (CP) procedure was used to eliminate the effect of the native oxide film on the Mg sample on contact angle measurements that is especially pronounced in conventional contact heating measurements with liquid metals sensitive to oxidation (Ref 28-30). This procedure involves non-contact heating of a couple of materials to a given temperature above the melting point of the metal sample combined with its mechanical cleaning from the native oxide film by squeezing the metal drop through a hole in the graphite capillary (Note: All happens in situ, directly at high temperature in the measurement chamber (Ref 28-30)). In addition, compared to traditional contact heating, the CP procedure allows for obtaining a symmetrical liquid metal drop. After deposition of the liquid Mg drop on the Ag substrate at $T_{exp}$, the resulting Mg/Ag couple was held at the measurement temperature for about 60 s.

The images of the Mg/Ag couples were recorded with two high-resolution CCD cameras at 57 frames per second during the measurements. These cameras are placed perpendicular to each other, which makes it possible to check the symmetry of the drop, position the liquid drop in the center of the substrate and observe very accurately the high-temperature phenomena occurring at the drop-substrate interaction (Ref 28). Images captured from one of the cameras (Ref 28) were used to determine the left, right, and average values of the contact angle ($\theta_l$, $\theta_r$, $\theta_{av}$, respectively) by means of DROP software, originally designed for this purpose (Ref 31).

### 2.2 Microstructure Observations

Once wettability measurements were completed, the solidified Mg/Ag couple was subjected to top-view observations using an FEI E-SEM XL30 Scanning Electron Microscope (SEM) integrated with an energy-dispersive x-ray spectrometer EDAX GEMINI 4000 (EDS). Microstructure observations and chemical composition analyses were conducted at an accelerating voltage of 20 kV and a spot size of 4.5 $\mu$m, as well as a working distance of

10 $\mu$m. Microstructures were recorded at magnifications ranging from $\times$ 50 to $\times$ 10 000. In the first place, SEM analysis of the top-view of the sample obtained after high-temperature tests was made. Next, the same SEM/EDS analysis was performed on a cross-section of the Mg/Ag coupled image perpendicular to the Mg/Ag interface. For this, a metallographic sample was prepared

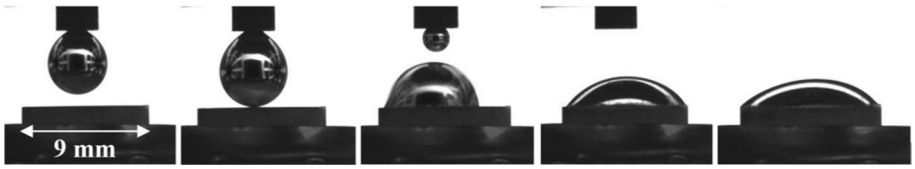


**Fig. 2** Images recorded of Mg/Ag couple by the monochromatic CCD camera during the sessile drop test by the CP procedure (720 °C/Ar + 5 wt.% $H_2$); the last image represents the end of the test after about 50 s

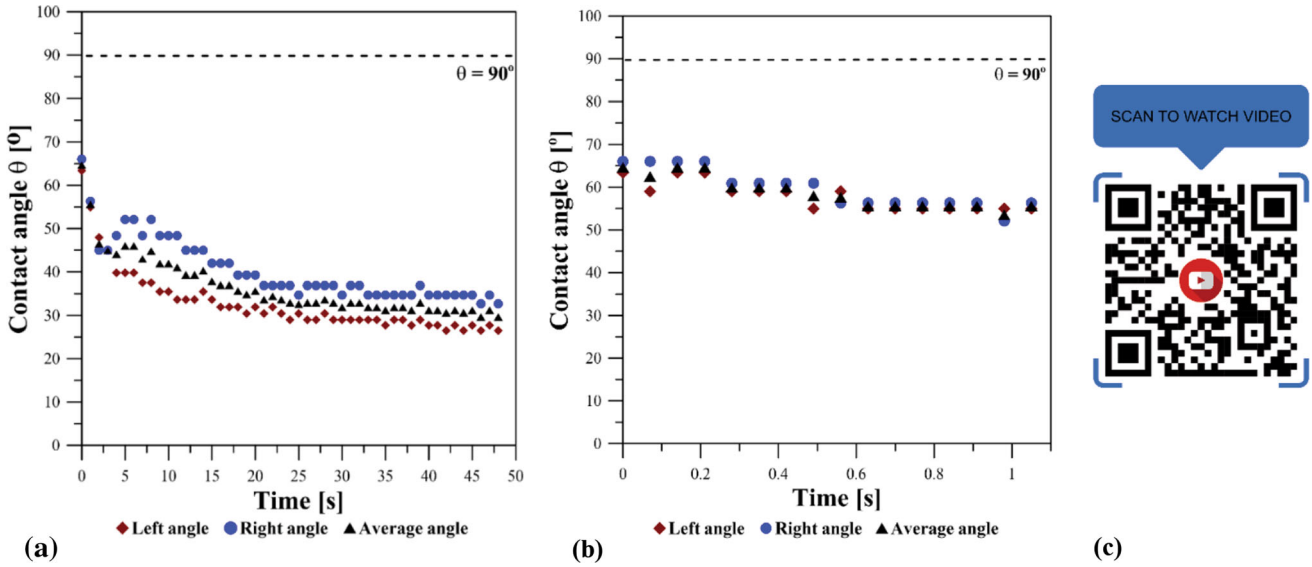


**Fig. 3** Wetting kinetics of liquid Mg on the Ag substrate registered during the sessile drop test by the CP procedure (720 °C/Ar + 5 wt.% $H_2$). (a) for 50 s, (b) for the first 1 s, (c) QR code for real-time video of the wettability test

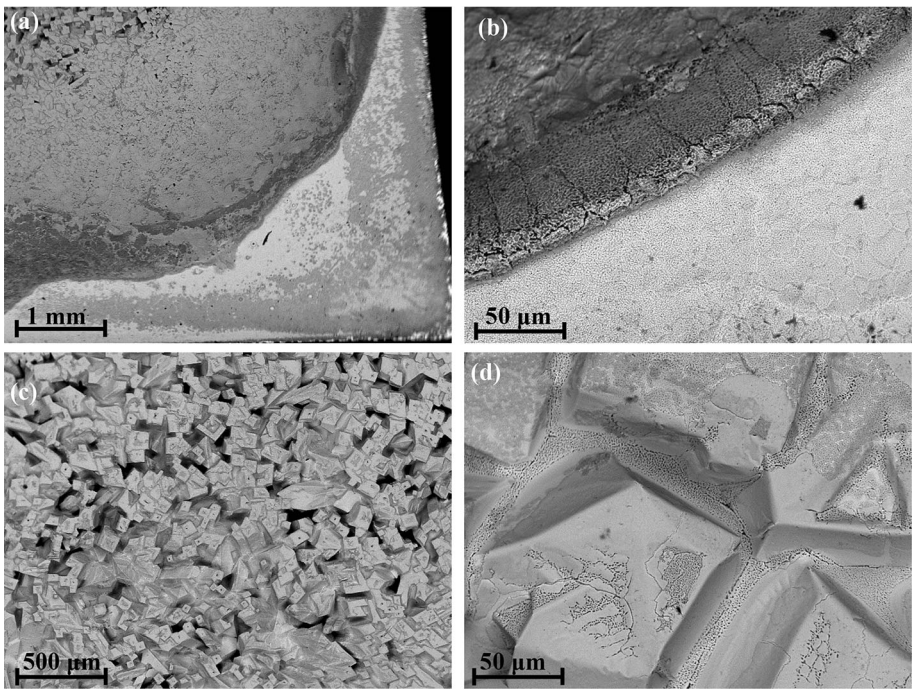


**Fig. 4** SEM top-view images showing different regions of Mg/Ag couple after wettability test: (a) in the vicinity of the triple line; (b) magnified region of (a); (c), (d) drop surface under different magnification

from the Mg/Ag couple by immersing it in a thermosetting epoxy resin and cut in half. Then, the cross-section of the sample was polished on sandpapers with gradations from 200 to 7000 and using 3-1/4 $\mu$m anhydrous diamond and $Al_2O_3$ suspensions. A thin layer of amorphous carbon (about 20-50 nm) was deposited on the surface of the obtained metallographic specimen to secure good electrical conductivity during SEM observations, as well as to avoid oxidation of the sample.

## 3. Results and Discussion

Selected images of the liquid Mg/Ag couple, corresponding to crucial stages of the sessile drop test accompanied with the capillary purification procedure (drop squeezing, drop deposition, detachment of the graphite capillary from the drop, the end of the test), recorded during holding at 720 °C in Ar + 5 wt.% $H_2$ atmosphere, are shown in Fig. 2.

For the liquid Mg/Ag couple, the wetting kinetics curves (the change in $\theta_l$, $\theta_r$, $\theta_{av}$ values versus time), as registered during the high-temperature wettability test at a temperature of 720 °C for 50 s, are presented in Fig. 3a and b. Calculations of contact angle values performed at 1 s intervals are presented in Fig. 3a, while those for the first second of contact at 0.1 s intervals are shown in Fig. 3b. The real-time video of the wettability test can be seen by scanning on QR code shown in Fig. 3c.

The first contact angle formed by the Mg drop after its deposition on the Ag substrate was less than 90°, thus showing a wetting phenomenon (for time $t$ = 0 s, $\theta_{av}$ = 65°) followed by

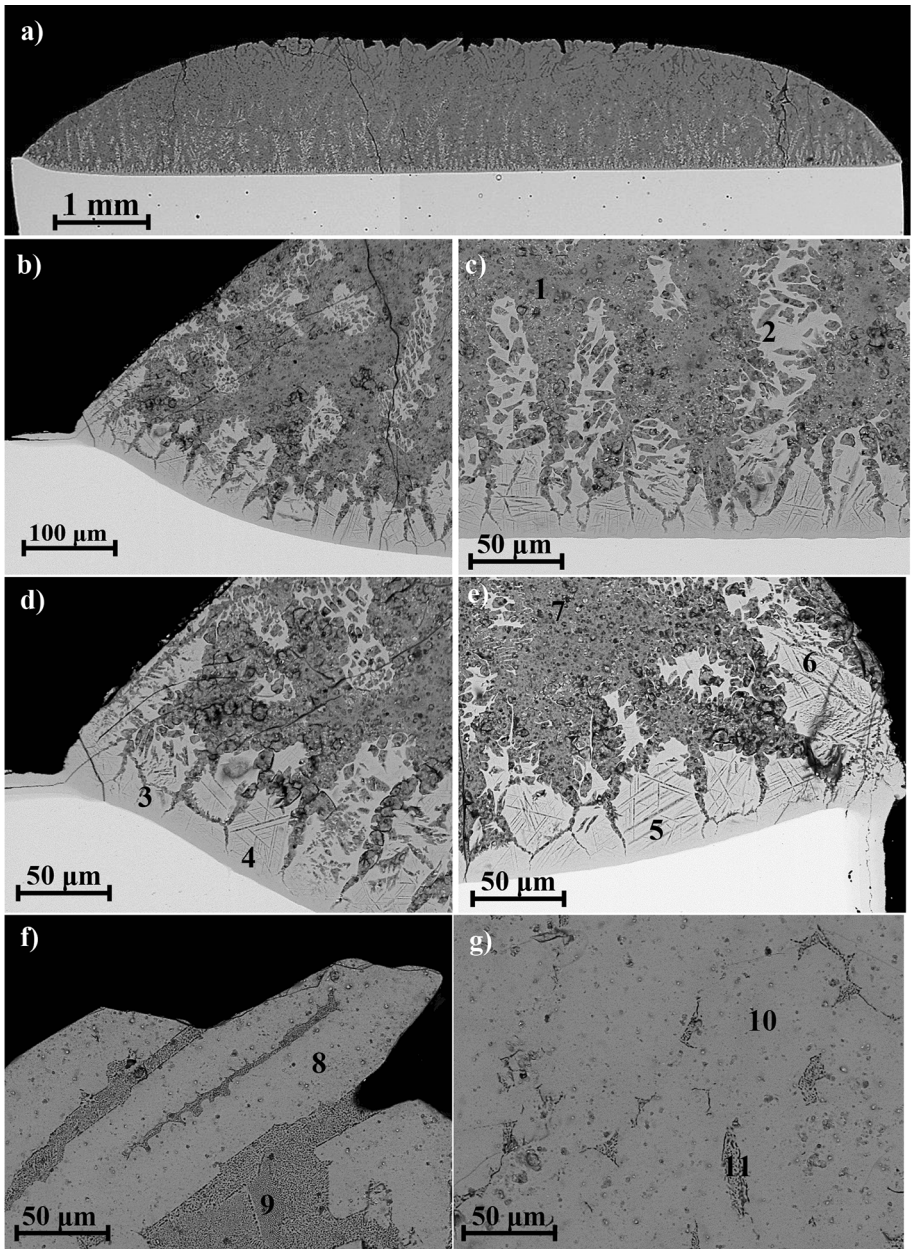


**Fig. 5** SEM images of cross-sectioned Mg/Ag couple made with a BSE detector at different magnifications: a) general view ( ×50); b) left side near the triple point ( ×500); c) interface in the central part of the drop; d, e) left and right drop edges; f) near the top surface of the drop; g) in the drop central part; (d)-(f) magnification × 1000

fast spreading over the substrate and continuous decrease of the contact angle up to the value of $\theta_{av} \sim 35°$ in 20 s. Further holding the couple at the test temperature resulted in only a slight change of the contact angle and after about 25 s, the $\theta_{av}$ values stabilized at the final value of 31°. The small variations in contact angle values seen in the points in Fig. 3 (especially for $\theta_r$) are attributed to the oscillation of the Mg drop and its spreading after deposition on the Ag substrate.

Structural characterizations of the solidified couple (Fig. 4 and 5) showed at good wetting and fast spreading of the Mg drop on the Ag substrate, which is related with a strong chemical interaction between them. Top-view SEM observations (Fig. 4a, b, c and d) revealed that the surface of the initially pure Mg drop had a heterogeneous structure. In the central part of the drop, its surface is covered with a large number of course crystals having a regular shape (Fig. 4c). These crystals were grown from the drop and they are surrounded with two-phase areas whose structure suggests eutectic constituent of the drop (Fig. 4d). Similar two-phase regions can be distinguished on the top surface of large crystals. It suggests that these crystals were formed as the first solidified phase which was well wettable by the residual eutectic constituent of the liquid drop, solidified as the last one. In the vicinity of the triple line, the presence of a halo around the drop on the substrate surface is well distinguished (Fig. 4a). Its observation under higher magnification (Fig. 4b) reveals two rings of dissimilar structure. The first ring of a smooth surface is next to the drop, while the second outer ring has a rough surface.

The representative results of SEM observations of the cross-sectioned Mg/Ag couple (Fig. 5) reveal three important features of a strong interaction between the Mg drop and the Ag substrates:

1) A deep crater ($\sim 200\ \mu$m) in the substrate under the drop due to the dissolution of Ag in liquid Mg. The formation of such a crater of sigmoidal interface profile may suggest that the contact angles, calculated from the side-view sessile drop images, are apparent (32), while the real final contact angles $\theta_l$ and $\theta_r$ in the Mg/Ag couple, which can be determined from the SEM image of cross-sectioned sessile drop sample, can be almost two times larger (Fig. 5b and c for $\theta_l$ and $\theta_r$, respectively). Moreover, there are two additional phenomena that might also affect the real values of $\theta_l$ and $\theta_r$, i.e. during isothermal heating of the Mg/Ag couple at the test temperature, it is unavoidable magnesium evaporation (Ref 28, 32), resulting in a decrease of the drop volume and pinning effect (Ref 32), while during solidification, it is the drop shrinkage observed in our test.

2) Multiphase composition of the initially pure Mg drop after its solidification due to alloying of liquid Mg with Ag. The structure of the solidified drop is composed of a large number of white primary crystals, surrounded with eutectic constituent and showing well-distinguished directional solidification perpendicular to the substrate surface, i.e. accordingly to the heat transfer.

3) A continuous layer of a new phase of a white color formed at the Mg/Ag interface and growing behind the triple line as can be seen on the left and right edges of the drop in Fig. 5b c, respectively.

It should be highlighted that SEM observations were performed on the solidified sessile drop couple of which structure was strongly affected by the cooling and solidification history. Therefore, for clarification of the main steps of high-temperature interaction taking place between liquid Mg drop and the Ag substrate during the wettability test, the detailed EDS characterization of the cross-sectioned Mg/Ag couple (Table 1) was assisted with the analysis of the Mg-Ag phase diagram (Fig. 6), calculated with the use of FactSage software and FTlite database (Ref 33). The main findings can be summarized as follows. It is believed that the first contact angle, measured at the time $t = 0$ s, corresponds to the contact angle formed by pure Mg on the Ag substrate. Next, the dissolution of Ag in liquid Mg takes place because, at the test temperature of 720 °C, liquid Mg can dissolve about 35 at.% Ag. It results in a decrease of the contact angle and a fast drop spreading over the Ag substrate through a dissolutive wetting mechanism. The final stage of the interaction between the Ag substrate and the Mg drop, saturated with Ag upon isothermal heating at the test temperature, is accompanied with the formation of and growth of a continuous light gray layer at the Mg/Ag interface (points 2-6 in Fig. 5c,d and e). The results of EDS analyses at selected points of this layer showed that it consists of an average of 49 at.% Mg and 51 at.% Ag. Moreover, this layer covers the substrate surface outside the wetting front (well distinguished as a halo around the drop, point 3 in Fig. 5d) because the surface diffusion is orders of magnitude faster than the diffusion in a bulk. Thus, the final stage of interaction corresponds to a slight improvement of wetting through the formation of the interfacial reaction product.

During cooling, the following stages can be identified, according to the Mg-Ag phase diagram shown in Fig. 6. First, with a decrease in temperature, the dissolution of Ag in liquid Mg decreases and it results in heterogeneous nucleation and growth of β-MgAg phase at the surface of already formed AgMg interfacial layer. The results of EDS analyses at selected points showed that the light gray phase consists of an average of 49 at.% Mg and 51 at.% Ag, while the dark gray phase consists of ~ 71 at.% Mg and 29 at.% Ag (Fig. 5c, d, e, f and g points 1-11, Table 1). These findings clearly indicate the mutual dissolution of the contacted drop/substrate couple.

In other words, the interfacial layer of the β-MgAg phase shown in Fig. 5 is composed of two sublayers of which the first one of homogeneous thickness was reactively formed at the substrate-side interface at the test temperature while the second one was formed at the drop-side interface during cooling. The second sublayer has a morphology typical for the solidification stage, i.e. scallop-like structure with light gray crystallites

**Table 1 Results of EDS analysis of phases marked in Fig. 5c, d, e, f and g**

| | Composition in marked points | | |
|---|---|---|---|
| Point no | Mg, at.% | Ag, at. % | Possible phases |
| 1 | 71.7 | 28.3 | ε-$AgMg_3$ |
| 2 | 50.9 | 49.1 | β-AgMg |
| 3 | 51.2 | 48.8 | β-AgMg |
| 4 | 49.1 | 40.9 | β-AgMg |
| 5 | 48.0 | 52.0 | β-AgMg |
| 6 | 45.5 | 54.5 | β-AgMg |
| 7 | 66.5 | 33.5 | ε-$AgMg_3$ |
| 8 | 72.5 | 27.5 | ε-$AgMg_3$ |
| 9 | 79.2 | 20.8 | $((Mg) + AgMg_4)_{eut}$ |
| 10 | 72.4 | 27.6 | ε-$AgMg_3$ |
| 11 | 77.8 | 22.8 | $((Mg) + AgMg_4)_{eut}$ |

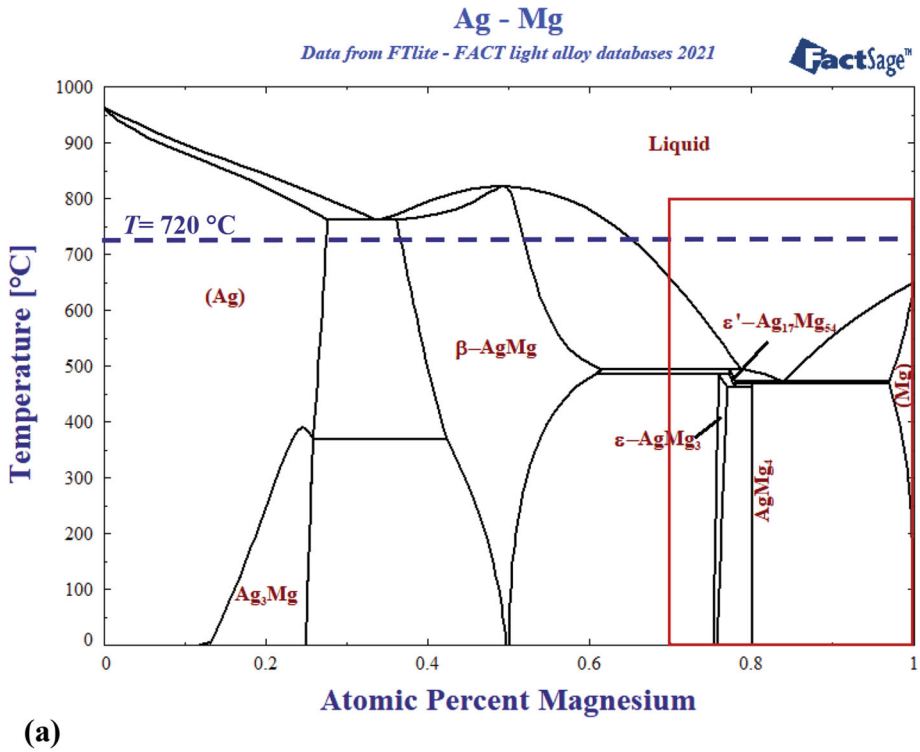


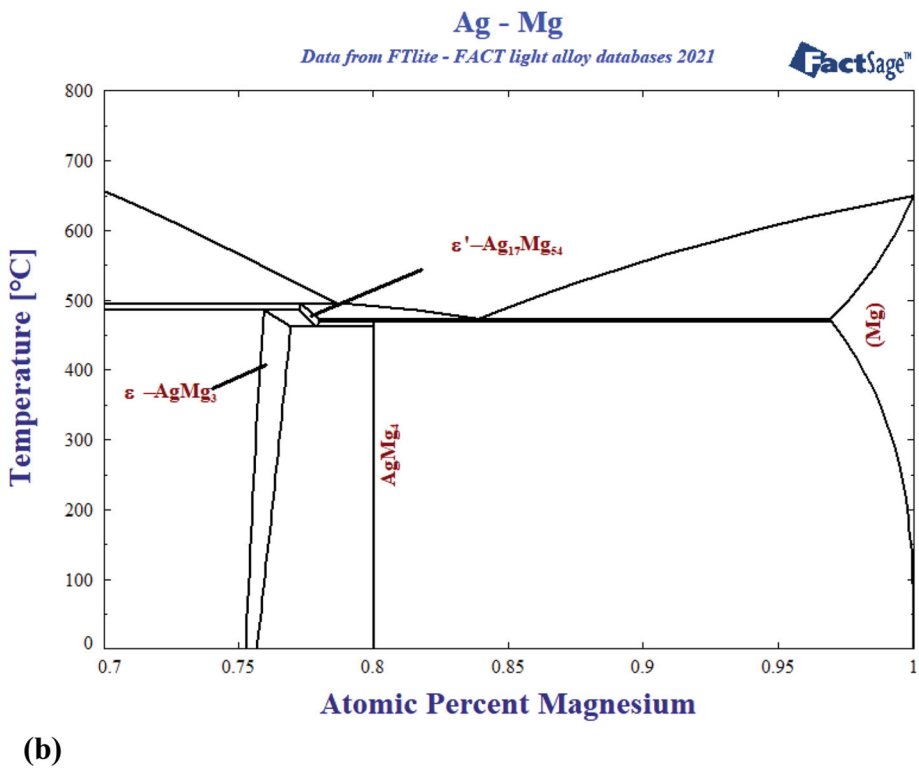


**Fig. 6** Phase diagram of the Ag-Mg system calculated with the use of FactSage software and FTlite database (Ref 33); the insert in (a) corresponds to the magnified Mg-rich region shown in (b)

positioned and grown towards the top of the drop. This phase has a large temperature-dependent solubility range (Fig. 6) and forms characteristic long crystallites through directional crystallization. Between these crystals, a second phase with a varied structure is observed (Fig. 5).

This solidification stage is accompanied with the change of Mg-Ag drop composition because Ag dissolved in the drop is partially consumed for the formation of the β-AgMg phase. From the Mg-Ag phase diagram, we may expect that during the next stage of cooling, the β-AgMg phase can be partially

transformed to ε′-$Ag_{17}Mg_{54}$ phase, because of peritectic reaction at a temperature of 494 °C:

$$L + \beta - AgMg \rightarrow \varepsilon' - Ag_{17}Mg_{54} \quad \text{(Eq 1)}$$

Despite the fact that we have no clear evidence of the formation of the ε′-$Ag_{17}Mg_{54}$ phase, we believe that the unusual shape of the β-AgMg crystals, located far from the interface, suggests their partial disappearance due to a process similar to a peritectic reaction (Figs. 5c, d and e). Particularly, it is well distinguished in Fig. 5e showing fragmentation of the β-AgMg crystals that took place in still molten Mg-Ag drop. From the Mg-Ag phase diagram (Fig. 6), the ε′-$Ag_{17}Mg_{54}$ phase can be transformed to ε-$AgMg_3$ because the ε′-phase exists in a narrow temperature range.

In the next stage, the dissolution of Ag in molten Mg continuously decreases with a decrease in temperature and it is accompanied with the nucleation and growth of the ε-$AgMg_3$ phase in the form of dark gray large crystals at the top of the drop and smaller crystallites inside the drop (∼ 71 at.% Mg and ∼ 29 at.% Ag; points 1, 7, 8, and 10 in Fig. 5).

According to the course of the liquidus line, the final stage of solidification at a temperature of ∼ 470 °C is related to the eutectic transformation of the Mg-Ag melt to form a two-phase eutectic mixture (Mg) + $AgMg_4$:

$$L(Mg - Ag) \rightarrow AgMg_4 + (Mg) \quad \text{(Eq 2)}$$

Following SEM observations, the eutectic (Mg) + $AgMg_4$ is mostly located in the center of the solidified drop and at the top between the crystals of the ε-phase.

## 4. Conclusions

For the first time, the high-temperature interaction of liquid pure magnesium with solid silver was examined experimentally using the sessile drop method combined with non-contact heating and in-situ cleaning of Mg drop from native oxide film by the capillary purification procedure.

Under the conditions of this study, immediately after contact with the Ag substrate, liquid oxide-free Mg drop showed good wetting and fast spreading over the substrate to form the final contact angle of ∼ 31°. However, this value should be considered as an apparent one because of the formation of a deep crater (200 $\mu$m) in the substrate under the drop due to the dissolution of Ag in the Mg drop. The SEM/EDS analysis of cross-sectioned couples evidenced the presence of a continuous layer of intermetallic phase (β-AgMg) at the Mg/Ag interface while the structure of initially pure Mg drop changed to that of Mg-Ag alloy.

Structural observations show a good agreement with the Ag-Mg phase diagram: the first-phase β-AgMg forms a continuous layer of varying chemical composition due to its large solubility range, depending on the temperature. In the final stage of drop solidification, according to the course of the liquidus line, a eutectic (Mg) + $AgMg_4$ is formed between the crystals of the ε-phase and in the central part of the solidified drop.

Comparison of the results of structural observations with the Mg-Ag phase diagram suggests that a very good wetting and fast spreading observed experimentally for the Mg/Ag couple is caused by high reactivity between liquid Mg and Ag substrate leading to the combined effect of two reactive wetting mechanisms, i.e. through dissolutive wetting and wetting through the formation of the interfacial reaction product, most likely the β-AgMg phase.


## Acknowledgements

This research was supported by the National Science Centre of Poland within OPUS 21 Project, no. 2021/41/B/ST5/02787. This paper received the Best Poster Award of the Polish Materials Science Society (PTM) at the 10th International Conference on High Temperature Capillarity organized in 2022 in Kraków, Poland.


## Conflict of interest

The authors declare that they have no known competing financial interests or personal relationships that could have appeared to influence the work reported in this paper.



## References


1. Y.-H. Ho, H.D. Vora, and N.B. Dahotre, Laser Surface Modification of AZ31B Mg Alloy for Bio-Wettability, *J. Biomater. Appl.*, 2015, **29**(7), p 915–928. https://doi.org/10.1177/0885328214551156
2. F. Witte, V. Kaese, H. Haferkamp, E. Switzer, A. Meyer-Lindenberg, C.J. Wirth, and H. Windhagen, In Vivo Corrosion of Four Magnesium Alloys and the Associated Bone Response, *Biomaterials*, 2005, **26**, p 3557–3563. https://doi.org/10.1016/j.biomaterials.2004.09.049
3. M.P. Staiger, A.M. Pietak, J. Huadmai, and G. Dias, Magnesium and its Alloys as Orthopedic Biomaterials: A Review, *Biomaterials*, 2006, **27**(9), p 1728–1734. https://doi.org/10.1016/j.biomaterials.2005.10.003
4. J.M. Banovetz, P. Sharp, R.A. Probe, and J.O. Anglen, Titanium Plate Fixation: A Review of Implant failures, *J. Orthopaed. Trauma*, 1996, **10**, p 389–394. https://doi.org/10.1097/00005131-199608000-00005
5. L. Li, J. Gao and Y. Wang, Evaluation of Cyto-Toxicity and Corrosion Behavior of Alkali-Heat-Treated Magnesium in Simulated Body Fluid, *Surf. Coat. Technol.*, 2004, **185**(1), p 92–98. https://doi.org/10.1016/j.surfcoat.2004.01.004
6. K. Bryla, J. Horky, M. Krystian, L. Litynska-Dobrzynska, and B. Mingler, Microstructure, Mechanical Properties, and Degradation of Mg-Ag Alloy After Equal-Channel Angular Pressing, *Mat. Sci. Eng. C.*, 2020, **109**, p 110543. https://doi.org/10.1016/j.msec.2019.110543
7. D. Raftopoulos, E. Katsamanis, F. Saul, W. Liu, and S. Saddemi, An Intermediate Loading Rate Technique for the Determination of Mechanical Properties of Human Femoral Cortical Bone, *J. Biomed. Eng.*, 1993, **15**, p 60–66. https://doi.org/10.1016/0141-5425(93)90095-G
8. E. Zhang, D. Yin, L. Xu, L. Yang, and K. Yang, Microstructure, Mechanical and Corrosion Properties and Biocompatibility of Mg–Zn–

Mn Alloys for Biomedical Application, *Mater. Sci. Eng. C.*, 2009, **29**, p 987–993. https://doi.org/10.1016/j.msec.2008.08.024
9. M.M. Zerankeshi and R. Alizadeh, Ag-Incorporated Biodegradable Mg Alloys, *Materialia*, 2022, **23**, p 101445.
10. K. Indira, C. Sylvie, W. Zhongke, and Z. Hongyu, Investigation of Wettability Properties of Laser Surface Modified Rare Earth Mg Alloy, *Proc. Eng.*, 2016, **141**, p 63–69. https://doi.org/10.1016/j.proeng.2015.08.1106
11. D. Tie, F. Feyerabend, W.D. Müller, R. Schade, K. Liefeith, K.U. Kainer, and R. Willumeit, Antibacterial Biodegradable Mg-Ag Alloys, *Eur. Cell. Mater.*, 2013, **25**, p 284–298.
12. R.C. Zeng, W. Dietzel, F. Witte, N. Hort, and C. Blawert, Progress and Challenge for Magnesium Alloys as Biomaterials, *Adv. Eng. Mater.*, 2008, **10**, p B3–B14. https://doi.org/10.1002/adem.200800035
13. B. Zberg, P.J. Uggowitzer, and J.F. Loffler, MgZnCa Glasses Without Clinically Observable Hydrogen Evolution for Biodegradable Implants, *Nat. Mater.*, 2009, **8**, p 887–891. https://doi.org/10.1038/nmat2542
14. H.M. Wong, K.W.K. Yeung, K.O. Lam, V. Tam, P.K. Chu, K.D.K. Luk, and K.M.C. Cheung, A Biodegradable Polymer-Based Coating to Control the Performance of Magnesium Alloy Orthopedic Implants, *Biomaterials*, 2010, **31**, p 2084–2096.
15. Y.C. Xin, J. Jiang, K.F. Huo, G.Y. Tang, X.B. Tian, and P.K. Chu, Corrosion Resistance and Cytocompatibility of Biodegradable Surgical Magnesium Alloy Coated with Hydrogenated Amorphous Silicon, *J. Biomed. Mater. Res. A*, 2009, **89A**, p 717–726.
16. Y. Ren, H. Zhao, L. Wang, B. Yang, H. Li, S. Sun, H. Pan, and G. Qin, Evidence of a Novel Intermetallic $Mg_7Ag_3$ Phase in Mg–Ag Binary Alloy System, *J. Appl. Cryst.*, 2018, **51**, p 844–848. https://doi.org/10.1107/S160057671800599X
17. P.S. Murphy and G.R.D. Evans, Advances in Wound Healing: A Review of Current Wound Healing Products, *Plast. Surg. Int.*, 2012, **2012**, p 190436. https://doi.org/10.1155/2012/190436
18. W. Chen, Y. Liu, H.S. Courtney, M. Bettenga, C.M. Agrawal, J.D. Bumgardner, and J.L. Ong, In Vitro Anti-Bacterial and Biological Properties of Magnetron co-Sputtered Silver-Containing Hydroxyapatite Coating, *Biomaterials*, 2006, **27**, p 5512–5517. https://doi.org/10.1016/j.biomaterials.2006.07.003
19. W.H. Song, S.R. Hyun, and S.H. Hong, Antibacterial Properties of Ag (or Pt)-Containing Calcium Phosphate Coatings Formed by Micro-Arc Oxidation, *J. Biomed. Mater. Res. Part A.*, 2009, **88**, p 246–254. https://doi.org/10.1002/jbm.a.31877
20. P.S. Brunetto, T.V. Slenters, and K.M. Fromm, In Vitro Biocompatibility of New Silver(I) Coordination Compound Coated-Surfaces for Dental Implant Applications, *Materials*, 2010, **4**, p 355–367. https://doi.org/10.3390/ma4020355
21. K. Jähn, H. Saito, H. Taipaleenmäki, A. Gasser, N. Hort, F. Feyerabend, H. Schlüter, J.M. Rueger, W. Lehmann, R. Willumeit-Römer, and E. Hesse, Intramedullary Mg2Ag Nails Augment Callus Formation During Fracture Healing in Mice, *Acta Biomater.*, 2016, **36**, p 350–360. https://doi.org/10.1016/j.actbio.2016.03.041
22. B.E. Paton, D.M. Kaleko, Y.M. Koval, V.M. Slipchenko, R.Y. Musienko, L.M. Neganov, V.V. Odnosum, and T.G. Sych, Influence of Alloying with Silver and Tantalum on Features of Medical-Purpose Ti-Ni Alloy, *Metallofiz. Nov. Tekhnol Met. Phys. Adv. Techn.*, 2010, **32**, p 1691–1703.
23. C.F. Huang, H.J. Chiang, W.C. Lan, H.H. Chou, K.L. Ou, and C.H. Yu, Development of Silver-Containing Austenite Antibacterial Stainless Steels for Biomedical Applications Part I: Microstructure Characteristics, Mechanical Properties and Antibacterial Mechanisms, *Biofouling*, 2011, **27**, p 449–457. https://doi.org/10.1080/08927014.2011.582642
24. B.S. Necula, I. Apachitei, F.D. Tichelaar, L.E. Fratila-Apachitei, and J. Duszczyk, An Electron Microscopical Study on the Growth of $TiO_2$-Ag Antibacterial Coatings on $Ti_6Al_7Nb$ Biomedical Alloy, *Acta Biomater.*, 2011, **7**, p 2751–2757. https://doi.org/10.1016/j.actbio.2011.02.037
25. M. Bosetti, A. Massè, E. Tobin, and M. Cannas, Silver Coated Materials for External Fixation Devices: In Vitro Biocompatibility and Genotoxicity, *Biomaterials*, 2002, **23**, p 887–892. https://doi.org/10.1016/S0142-9612(01)00198-3
26. J. Hardes, A. Streitburger, H. Ahrens, T. Nusselt, C. Gebert, W. Winkelmann, A. Battmann, and G. Gosheger, The Influence of Elementary Silver Versus Titanium on Osteoblast Behaviour in Vitro Using Human Osteosarcoma Cell Lines, *Sarcoma*, 2007, **2007**, p 026539. https://doi.org/10.1155/2007/26539
27. R. Karunakaran, S. Ortgies, A. Tamayol, F. Bobaru, and M.P. Sealy, Additive Manufacturing of Magnesium Alloys, *Bioact. Mater.*, 2020, **5**(1), p 44–54. https://doi.org/10.1016/j.bioactmat.2019.12.004
28. S. Terlicka, P. Darłak, N. Sobczak, and J.J. Sobczak, Non-Wetting and Non-Reactive Behavior of Liquid Pure Magnesium on Pure Tungsten Substrates, *Materials*, 2022, **15**(24), p 9024. https://doi.org/10.3390/ma15249024
29. N. Sobczak, M. Singh, and R. Asthana, High-Temperature Wettability Measurements in Metal/Ceramic Systems—Some Methodological Issues, *Curr. Opin. Solid State Mater. Sci.*, 2005, **9**, p 241–253. https://doi.org/10.1016/j.cossms.2006.07.007
30. A. Kudyba, N. Sobczak, W. Polakowski, G. Bruzda, A. Polkowska, and D. Giuranno, Improved Methodological Concepts for Processing Liquid Mg at High Temperature, *J. Magnes. Alloy.*, 2021, **9**(15), p 183–191. https://doi.org/10.1016/j.jma.2020.06.003
31. E. Ziółkowski, J.J. Sobczak, P. Fima, and N. Sobczak, Implementation of a Methodology for Determining the Density and Surface Tension of Liquid Metal During High-Temperature Tests, Metalurgia 2020, ISBN 978–83- 63605–51–3, 519–530
32. A. Passerone, F. Valenza, and M.L. Muolo, Wetting at high temperature Chapter XII, *Drops and bubbles in contact with solid surfaces*. M. Ferrari, L. Liggieri, R. Miller Ed., CRC Press, Progress in colloid and interface science, 2013, p 299–334
33. FactSage Version 8.2, with FTlite Database. Available online: https://www.crct.polymtl.ca/fact (accessed on 20 December 2022)